POST-WMAP ASSESSMENT OF INFRARED CUTOFF IN THE PRIMORDIAL SPECTRUM FROM INFLATION

Rita Sinha[*] and Tarun Souradeep[†]

Inter-University Center for Astronomy and Astrophysics,
Post Bag 4, Ganeshkhind Pune 411007 India.
(Dated: February 5, 2008)

The recent Cosmic Microwave Background (CMB) measurements indicate that there is power deficiency of the CMB anisotropies at large scales compared with the ΛCDM model. We have investigated the possibility of explaining such effects by a class of primordial power spectra which have infrared cutoffs close to the horizon scale. The primordial power spectrum recovered by direct deconvolution of the observed CMB angular spectrum indicates that the data prefers a sharp infrared cutoff with a localized excess (bump) just above the cutoff. We have been motivated to assess plausible extensions of simplest inflationary scenarios which readily accommodate similar form of infrared cutoff. We carry out a complete Bayesian analysis of the parameter space using *Markov Chain Monte Carlo* technique with such a class of primordial power spectra. We show that primordial power spectrum that have features such as an infrared cutoff followed by a subsequent excess in power give better fit to the observed data compared to a nearly scale-invariant power law or power spectrum with just a monotonic infrared cutoff. However, there is substantial room for improvement in the match to data and calls for exploration of other mechanisms that may lead to infrared cutoff even closer to that recovered by direct deconvolution approach.

PACS numbers: 98.80.Cq, 98.80.-k

I. INTRODUCTION

The Cosmic Microwave Background (CMB) is the most copious of all the isotropic backgrounds observed from radio to gamma rays. It has become the most important observational tool both for determining the global cosmological parameters and to understand the physics of the early universe. The concordant model of cosmology that has emerged from recent observations is the inflationary ΛCDM model. This describes the universe as spatially flat with primordial fluctuations which are adiabatic and Gaussian. The ΛCDM model has been quite successful in explaining many aspects of the universe conforming most with the observational data [1–4]. The primordial power spectrum formed during the inflationary epoch, in the simplest case can be described as a single inflaton field with a nearly scale-invariant Harrison-Zel'dovich spectrum expressed as $\mathcal{P}(k) \propto k^{n_s - 1}$, 'k' being the comoving wavenumber. However, inflationary scenarios readily accommodate significant departures from scale invariance [5–11]. Distortions in the shape of the initial power spectrum imprints characteristic scales on the form of $\mathcal{P}(k)$. The amount of such distortions manifested on the angular power spectrum and the scales at which they occur are strictly related to the nature of the primordial fluctuations and to the matter content of the universe. Careful analysis of all features of the CMB power spectrum put constraints on the entire parameter space. Recently a lot of attention has been devoted to the power anomalies at low multipoles [12] compared to that obtained using the ΛCDM model of the universe. This was first reported by the Cosmic Background Explorer (COBE) [13] satellite and now further confirmed by Wilkinson Microwave Anisotropy Probe (WMAP) observations [2, 14, 15]. In the recent past many speculations have been made to provide a satisfactory explanation to this discrepancy but they have been successful only to a certain extent. The WMAP team have crudely fit the power at low scales by putting a running spectral index to the nearly scale-invariant power law [14]. This aspect has also been projected as a probable new feature in the CMB anisotropies such as related to curvature scale [16]. This has been related to the topology of the universe as well, such as a dodecahedral universe [17] or possibly a violation of statistical isotropy [18]. A low quadrupole moment has been suggested to be originating also from dark energy, quintessence models with isocurvature perturbations [19, 20] via correlations with adiabatic density fluctuations which lower the adiabatic Integrated Sachs-Wolfe contributions to the quadrupole. Even model-independent searches have been made to look for features in the CMB power spectrum [21–25]. The studies where the power spectrum has been reconstructed in a set of bins in k-space have the obvious disadvantage that the reconstruction depends on the width and the placement of the bins. This is also true for methods

---

[*]Electronic address: `rsinha@iucaa.ernet.in`
[†]Electronic address: `tarun@iucaa.ernet.in`

such as linear interpolation, wavelet, top-hat bins which can contribute to smoothening out or omission of features. Despite the progress the issue of low scale power still remains a subject of debate. The most crucial point perhaps is the limited information available at large angular scales due to cosmic variance [26]. Although large cosmic variance at the quadrupole does make the power discrepancy less significant, it is important to bear in mind that cosmic variance is proportional to the 'true' angular power spectrum of the underlying model. The cosmic variance is small for a model that predicts the observed low quadrupole. In principle, the case for an infrared cutoff is best addressed by bayesian evidence study. However, different bayesian evidence studies for the models with infrared cutoff has yielded different conclusions regarding the evidence for an infrared cutoff in the primordial spectrum [28, 29]. This is possibly due to the dependence of bayesian evidence analysis on the different class of models explored, details of parameterization of models and the datasets used. Hence these results may not readily translate into a general conclusion on the evidence for 'infrared cutoff' though [28] find that models with cutoff in power generally produce higher evidence compared to scale invariant or a single spectral index model.

We revisit the possibility of explaining this observed suppression of power at low multipoles using known mechanisms of modifying the shape of the primordial power spectrum from inflation to introduce an infrared cutoff [30–33]. The limited success of model spectra with monotonic infrared cutoff studied is apparent from the non-monotonic infrared cutoff indicated by direct deconvolution of the primordial spectrum from the CMB angular power spectrum using WMAP data [24, 34]. The direct approach suggests that the data favours a sharp infrared cutoff followed by a localized excess ('bump'). As mentioned in Ref. [24], this is not uncommon since mechanisms that produce a sharp change in amplitude (such as required for the infrared cutoff) can also have an overshoot followed by damped oscillations [35]. Here, we focus on inflationary models with an infrared cutoff followed by a localized excess power (referred to as 'bump') in the power spectrum as a feasible possibility in explaining this deviation. This seems to be a promising avenue (such as [36]). Such features have also been seen by large-scale structure surveys [13, 34, 37, 38]. We have carried out an exhaustive parameter estimation with such a class of primordial spectra using the Bayesian approach by applying the *Markov Chain Monte Carlo* (MCMC) technique [39].

In the sections to follow we first describe briefly in section II, the various forms of primordial power spectra considered in this study. This is followed in section III by a brief overview of the methodology adopted (MCMC). In Section IV we give the parameter estimates with such a class of primordial power spectra which is followed by the final section on discussion and conclusion.

II. PRIMORDIAL POWER SPECTRA WITH FEATURES

While reconstructing the initial conditions of the universe it is important to devise a method that can efficiently constrain the shape of the power spectrum of primordial matter density fluctuations. It has been shown in [24] that the direct recovery of the primordial power spectrum from the CMB (WMAP) observations indicate a sharp infrared cutoff around the horizon scale ($k_* \sim k_h = 2\pi/\eta_0$, where η_0 is the present horizon) followed by a 'bump' [40]. The resulting angular spectrum gives a significantly better likelihood than a simple (scale-invariant) Harrison-Zel'dovich, scale-free power spectrum and also a simple monotonic infrared cutoff. This motivates us to consider a broader variety of primordial power spectra with infrared cutoffs at low wavenumber arising from physics in the initial phase of a (limited) inflationary epoch.

In this section we describe such primordial power spectra with features which have been considered in this work and each model is motivated by some plausible inflationary scenario. Fig. 1 shows the best fit spectra for the class of primordial power spectra considered below.

A. Scale-free Power Law model-PL(I)

Before we go on to describe initial power spectra with features we would like to mention the commonly assumed power law power spectrum (referred to as 'Power Law' model here). This is generally parametrized in terms of the slow-roll approximation of the single-inflaton field and is given by

$$\mathcal{P}_o(k) = A_s \left(\frac{k}{k_0}\right)^{n_s-1}. \tag{2.1}$$

Here $n_s(k) = [d \ln \mathcal{P}(k)/dlnk] + 1$ is the scalar spectral index which is constant for power law models ($n_s = 1$ corresponds to a scale-invariant power spectrum) and k_0 is the scalar pivot scale. The power spectrum amplitude, A_s determines the variance of the fluctuations.

The various inflation motivated primordial power spectra models [41] with infrared cutoffs (with or without a 'bump') which have been explored in this work are described below.

B. Exponential Cutoff model-EC(II)

This model has a monotonic cutoff imposed on (multiplying) a scale-free power law spectrum. Such an infrared cutoff discussed and motivated by [30] leads to power spectrum of the form (referred to as 'Expo-cutoff' model here)

$$\mathcal{P}(k) = A_s \, k^{n_s-1} \left[1 - e^{-(k/k_*)^\alpha} \right]. \tag{2.2}$$

In previous analyses using this model in [30, 31] the value of the parameter α was fixed ($\alpha = 3.35$) to approximately mimic the sharpness of the cutoff in a specific scenario (See Kin.Dom model described later). In our work here we allow it to vary and obtain the best fit value. As discussed later, our results indicate that a larger value of α is preferred.

C. Starobinksy model-SB(III)

It was shown by Starobinsky [42] that if the effective scalar inflaton potential has a 'singularity' in the form of a sharp change in the slope (a 'kink'), it can create an infrared suppression in power spectrum of adiabatic perturbations at any chosen wavenumber k_* (referred to as 'Starobinsky' model here). The infrared cutoff is followed by the 'bump' that arises naturally as the first peak of a damped ringing. The effect of a kink (sharp change in the slope) at some point of the inflaton potential can be neatly expressed in terms of the analytic multiplicative transfer function applied on the underlying power spectrum $\mathcal{P}_o(k)$ as

$$\mathcal{P}(k) = \mathcal{P}_o(k) \, \mathcal{D}^2(y, R_*). \tag{2.3}$$

In the simpler form (SB) we restrict $\mathcal{P}_o(k)$ to be a simple power law. However, in general, $\mathcal{P}_o(k)$ can be of any form allowed by models of scalar field driven inflation. For example, in the later section we take it to be of an exponential form (Expo-Staro model). The transfer function

$$\mathcal{D}^2(y, R_*) = [1 - 3 \, (R_* - 1) \frac{1}{y} \left((1 - \frac{1}{y^2}) \sin 2y + \frac{2}{y} \cos 2y \right) + \frac{9}{2} (R_* - 1)^2 \frac{1}{y^2} (1 + \frac{1}{y^2}) \times$$
$$(1 + \frac{1}{y^2} + (1 - \frac{1}{y^2}) \cos 2y - \frac{2}{y} \sin 2y)], \tag{2.4}$$

with $y = k/k_*$. R_* is the ratio of the slope $dV/d\phi$ which dictates the shape of the power spectrum, $V(\phi)$ being the inflaton potential of the scalar field ϕ. The power spectrum $\mathcal{P}(k)$ in eq. 2.3 has a step-up like feature (going to larger k) for $R_* < 1$ and a step-down like feature for $R_* > 1$. An infrared cutoff is created when $R_* < 1$. This shape of the primordial power spectrum with a Starobinsky step not only mimics the sharp infrared cutoff but also subsequently produces the required localized excess in power (the 'bump'). We have carried out MCMC analysis and obtained best fit values for k_* and R_*.

D. Pre-inflationary Kinetic Domination model-KD(IV)

The observable inflationary epoch could be preceded by a period of fast rolling of the inflaton field ϕ leading to pre-inflationary phase of kinetic domination. The difference of the vacuum in the kinetic domination (fast rolling) phase relative to the inflationary phase would imprint a feature in the power spectrum at large scales corresponding to first modes that crossed out of the Hubble radius at the onset of inflation [30]. The feature is an infrared cutoff akin to that first shown by Vilenkin and Ford [43] for a radiation dominated pre-inflationary phase. If the scale corresponding to the current horizon exited the horizon very soon after the onset of inflation, then the feature could explain the observed suppression of power at the horizon scale. The form of primordial perturbations is given by (referred to as 'Kin. Dom.' model here)

$$\mathcal{P}(k) = \frac{H^2}{2\pi^2} k \, | \, A - B \, |^2 \tag{2.5}$$

where

$$A = \frac{e^{-ik/H}}{\sqrt{32 \, H/\pi}} \left[\mathcal{H}_0^{(2)} \left(\frac{k}{2H} \right) - \left(\frac{H}{k} + i \right) \mathcal{H}_1^{(2)} \left(\frac{k}{2H} \right) \right]$$
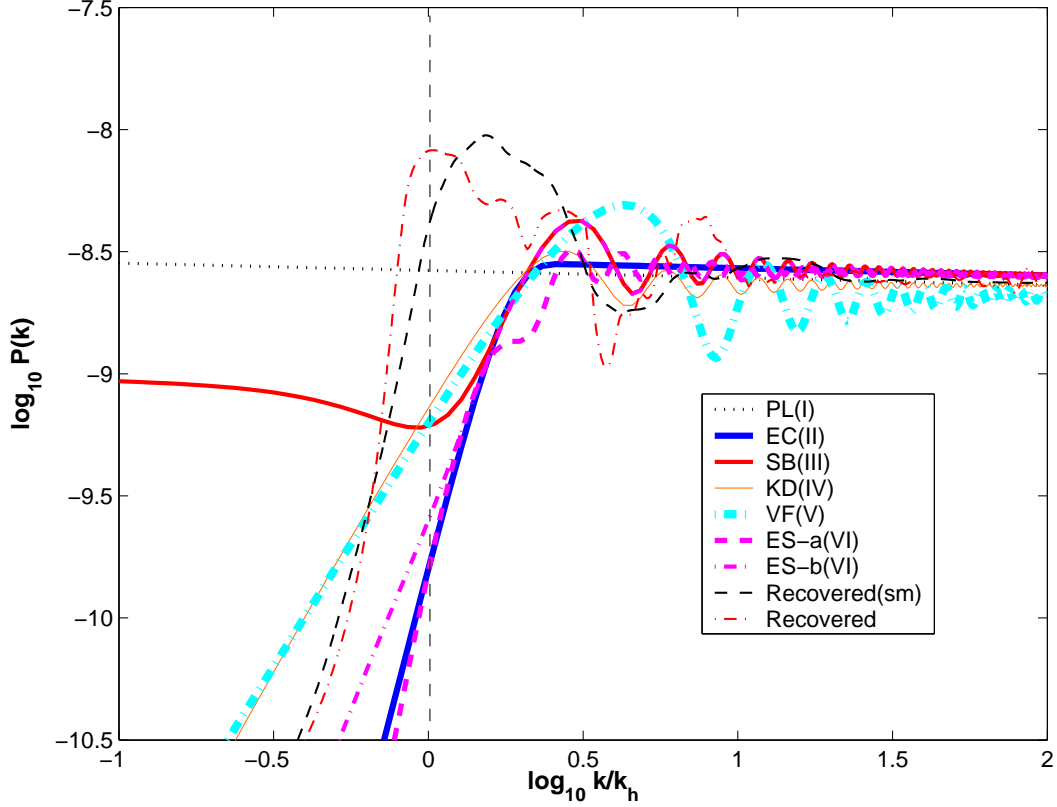
FIG. 1: The class of primordial power spectra with features which have been used in this work are plotted. Here $k_h = 2\pi/\eta_o \approx 4.5 \times 10^{-4}$ Mpc^{-1}, is the wavenumber corresponding to the Horizon scale for best fit ΛCDM model. For comparison we also give the power spectrum recovered from WMAP data by direct deconvolution [24] ('Recovered') and wavelet smoothed version that retains the most prominent features ('Recovered(sm)') (adapted from R. P. Manimaran *et al.*, *in preparation*). Notably, none of the model spectra are able to match up well to the form of infrared cutoff indicated by the direct deconvolution leaving room for further search of more likely inflationary scenario.

and

$$B = \frac{e^{ik/H}}{\sqrt{32\,H/\pi}} \left[\mathcal{H}_0^{(2)}\left(\frac{k}{2H}\right) - \left(\frac{H}{k} - i\right) \mathcal{H}_1^{(2)}\left(\frac{k}{2H}\right) \right].$$

Here H denotes the (physical) Hubble parameter during inflation while $\mathcal{H}_0^{(2)}$ and $\mathcal{H}_1^{(2)}$ denote the Hankel function of the second kind with order 0 and 1, respectively (for details refer to [30] and references therein).

E. Pre-inflationary Radiation domination model-VF(V)

For a pre-inflationary radiation dominated epoch the power spectrum was given by Vilenkin and Ford [43] as follows (referred to as 'VF' model here)

$$P(k) = A_s\, k^{1-n_s}\, \frac{1}{4y^4} \left| e^{-2iy}(1 + 2iy) - 1 - 2y^2 \right|^2, \tag{2.6}$$

where $y = k/k_*$. The VF power spectrum can also provide an infrared cutoff with the required 'bump' after it. The infrared cutoff here is not as sharp as the one arising from kinetic domination in the pre-inflationary phase and is found to be relatively disfavored in our work. The cutoff scale k_* is set by the Hubble parameter at the onset of inflation. Here too, the current horizon scale crosses the Hubble radius very close to the onset of inflation.

F. Exponential-Starobinsky model-ES(VI)

Encouraged by the reasonable success of the class of primordial spectra described in the earlier subsections we have undertaken a power estimation with yet another form of initial spectra tailored to mimic the cutoff and the 'bump' in the primordial power spectrum. As discussed earlier, the Starobinsky feature is a transfer function that modulates an underlying power spectrum expected from the inflaton potential without singularity and affects any inflationary scenario based on a inflaton potential with sharp change in slope (eq. 2.4). We imprint a Starobinsky break on an exponential cutoff spectrum (referred to as 'Expo-staro' model here) mainly motivated by the fact that these models provide a sharp reduction in large wavelength power needed to suppress the low multipoles of the CMB. The Expo-staro model has both the exponential cutoff providing an adjustable sharpness of the cutoff as well the bump of the Starobinsky feature and is more fine tuned as reflected by the additional parameter, ε_*. This can be described as

$$\mathcal{P}(k) \,=\, \mathcal{P}_o(k) \left[1 - e^{-(\varepsilon_* \, k/k_*)^{\alpha}} \right] \, \mathcal{D}^2(y, R_*) \,, \tag{2.7}$$

where $\mathcal{D}^2(y, R_*)$ is the transfer function of the Starobinsky feature described by eq.(2.4) and ε_* sets the ratio of the two cutoff scales involved (exponential cutoff and Starobinsky feature).

Using the recent measurement of the angular power spectrum of CMB anisotropy we undertake a full blown multi-parameter joint estimation of the parameters characterizing the infrared cutoff such as k_*, α and R_* (described above) together with the standard set of cosmological parameters. In the next section we briefly describe the parameter estimation method used in this work.

III. METHODOLOGY

Theoretical models for the determination of the power spectrum, which is responsible for structure formation, starts from the assumption of a primordial $\mathcal{P}_o(k)$ at a sufficiently high redshift $z \gg z_{eq}$, the redshift at matter-radiation equality. The primordial power spectrum is related to the linear CMB anisotropy power spectrum $C_l^{M_{12}}$ by the transfer function $T_l^{M_{12}}(k)$ such that [21]

$$C_l^{M_{12}} \,\propto\, \int \mathrm{d}\ln k \, \mathcal{P}(k) \, T_l^{M_1}(k) \, T_l^{M_2}(k) \tag{3.1}$$

where M_1 and M_2 are the indices for the temperature and the two polarization modes of the power spectra.

We use the well-known *Monte Carlo Markov Chain* (MCMC) technique [39, 44] to constrain the parameters with the observed data. Given a vector of cosmological data $\mathbf{d}$ (for instance, $\mathbf{d}$ can be the vector containing the 899 WMAP measurements of the temperature power spectrum C_l for $l = 2$ to 900) from which we want to measure a vector of cosmological parameters $\mathbf{p} \equiv (\tau, \Omega_m, \Omega_b, \Omega_\Lambda, k_*,...)$. The cosmological parameterization has been carried out in terms of the following parameters, namely, the baryon density $\Omega_b h^2$, cold dark matter density, $\Omega_{cdm} h^2$, Hubble constant H_o [45], and opacity to the surface of last scattering, τ [46]. Apart from these, we include the parameters characterizing the inflationary primordial perturbations with infrared cutoff features as described in the previous section (k_*, α, R_*) along with the scalar spectral index of perturbations, n_s [47] and the amplitude $\log[10^{10} A_s]$. We consider a flat universe with $\Omega_k = 0$. Table I gives the priors used in the study for the various inflationary and cosmological parameters. The ranges of these uniform priors have been varied to ensure that there is no dependence of priors on our results. We restrict our study to a cosmological flat model where the cosmological constant, $\Omega_\Lambda = 1 - \Omega_{cdm} - \Omega_b$ and do not consider other forms of dark energy. The theory $\mathbf{p}$ is connected to the data $\mathbf{d}$ by the likelihood function, $\mathcal{L}(\mathbf{p}, \mathbf{d})$, which gives the probability distribution for observing different $\mathbf{d}$ given a theoretical model $\mathbf{p}$ which in our case is the ΛCDM model. In Bayesian analysis, one inserts the actual observed data and and reinterprets $\mathcal{L}(\mathbf{p}, \mathbf{d})$ as an un-normalized probability distribution over the cosmological parameters $\mathbf{p}$, optionally after multiplication by a probability distribution, which has the prior information. To place constraints on any single parameter, one marginalizes (integrates) over all the others. In the MCMC method a large set of points $\mathbf{p}_i, i = 1$, ...n, i.e. a *Markov* chain, is generated by a stochastic procedure such that the points have a probability distribution $\mathcal{L}(\mathbf{p}, \mathbf{d})$. The basic MCMC algorithms used here are based on the Metropolis-Hastings and slice sampling methods. According to Metropolis-Hastings rule [49] higher likelihood trials are always accepted i.e. for $\mathcal{L}(\mathbf{p}_*, \mathbf{d}) > \mathcal{L}(\mathbf{p}_i, \mathbf{d})$, otherwise rejected and accepted only with probability $\mathcal{L}(\mathbf{p}_*, \mathbf{d})/\mathcal{L}(\mathbf{p}_i, \mathbf{d})$ where $\mathbf{p}_*$ is a new trial random point in the parameter space.

The other method used in the implementation of MCMC is slice sampling [39]. In slice sampling [50] similar to the Metropolis method the target density $\mathbf{p}_*(x)$ is evaluated at any point x. Here is a brief note

TABLE I: Uniform prior ranges for the parameters as used in the joint parameter estimation study.

	Parameter	Prior (range)
Baryon Density	$\Omega_b h^2$	0.005-0.1
Dark Matter Density	$\Omega_{dm} h^2$	0.01-0.99
Angular size of Acoustic Horizon[a]	θ	0.5-10.0
Optical Depth	τ	0.01-0.8
Scalar Spectral Index	n_s	0.5-1.5
Infrared Cutoff (wavenumber)	$k_* (\times 10^{-4})\mathrm{Mpc}^{-1}$	0.00001-0.0009
Expo Cutoff Steepness Parameter	α	0.1-10.0
Starobinsky Parameter	R_*	0.01-0.99
Amplitude Parameter[b]	$\log 10^{10} A_s$	2.7-4.0

[a]Acoustic horizon as defined in [45]
[b]Amplitude parameter as defined in [48]

on slice sampling algorithm. Consider a one-dimensional slice sampling method for making transitions from a two-dimensional point (x, u) lying under the curve $\mathbf{p}(x)$ to another point (x', u') lying under the same curve, such that the probability distribution of (x, u) tends to a uniform distribution over the area under the curve $\mathbf{p}_*(x)$, whatever initial point we start from. A single transition $(x, u) \to (x', u')$ of a one-dimensional slice sampling algorithm has the following basic steps. A vertical coordinate u' and an horizontal interval (x_a, x_b) enclosing x (i.e. a slice) is then drawn under the curve $\mathbf{p}_*(x)$. Now x' is drawn between this interval and $\mathbf{p}_*(x')$ is evaluated. If $\mathbf{p}_*(x') > u'$ then accept it otherwise choose a different interval and continue. There can be slight variations to this, for instance, 'stepping out' or 'shrinking' methods can be used for choosing the interval (x_a, x_b), the distribution under the curve always remaining uniform. Slice sampling is more robust to the choice of parameters like step sizes which is self tuning in this method and hence, we get better estimates when implementing MCMC with the new parameter set. However, slice sampling is slightly slower in terms of computer run-time.

We have evaluated the likelihood function $\mathcal{L}$ and obtained the best fit from the parameter searches using a modified version of CosmoMC [39]. We typically ran multiple chains on a 64 bit 8x4 Alpha-Server ES45 68/1250 System (1.25 GHz each) to optimize our parameter set. We have first conducted the analysis with only WMAP TT data wherein the discrepancy in power is more apparent. Later on the analysis has been extended to include both the WMAP TT and TE angular power spectra along with the CBI (Cosmic Background Imager), ACBAR (Arcminute Cosmology Bolometer Array Receiver) and VSA (Very Small Array) datasets of the CMB for small scales ($l \gtrsim 700$). These external datasets augment the quality of the analysis as well as help in alleviating parameter degeneracies. For instance, these are essential to break parameter degeneracy between the inflationary parameter, n_s and optical depth, τ. In addition, high resolution CMB datasets also help to tightly constrain the parameters for example, Ω_m, amplitude A_s, the running in the spectral index (not used here) [51–53].

IV. PARAMETER ESTIMATES

We have carried out a complete Bayesian analysis by varying and marginalizing over all the parameters considered in this work to obtain the best fit values. Table II and Table III sums the results of the MCMC simulations with the WMAP data only and WMAP data plus the addition of the external datasets, respectively. Tables II and III mention the values of some of the relevant parameters (the search has been made for a larger parameter space) along with their 1-σ error bars and their goodness-of-fit parameter ($\chi^2_{eff} \equiv -2 \ln \mathcal{L}$) values for the different models.

The best likelihood value (with the WMAP TT data) is given by ESa-b(VI) whereas EC(II) and SB(III)

TABLE II: Best fit values of parameters specifying the initial power spectrum (k_*, α, R_*, n_s) and other relevant cosmological parameters for a class of model power spectra with a infrared cutoff (dataset used: WMAP TT data).

Parameter	Expo-cutoff EC(II)	Starobinsky SB(III)	Kin. Dom. KD(IV)	VF VF(V)	**Expo-staro(a)[†] ES-a(VI)**	Expo-staro(b)[‡] ES-b(VI)	Power Law PL(I)
$k_*(\times 10^{-4})\mathrm{Mpc}^{-1}$	$3.0^{+4.8}_{-2.9}$	$3.1^{+5.8}_{-2.8}$	$3.5^{+3.0}_{-3.3}$	$0.4^{+0.7}_{-0.3}$	$\mathbf{3.0^{+0.5}_{-2.0}}$	$3.1^{+5.8}_{-2.1}$	$-$
α	$9.6^{+0.3}_{-8.6}$	$-$	$-$	$-$	$\mathbf{0.58^{+4.6}_{-0.43}}$	$0.72^{+9.1}_{-0.55}$	$-$
R_*	$-$	$0.73^{+0.25}_{-0.14}$	$-$	$-$	$\mathbf{0.17^{+0.80}_{-0.15}}$	$0.35^{+0.63}_{-0.20}$	$-$
n_s	$0.95^{+0.16}_{-0.03}$	$0.98^{+0.14}_{-0.07}$	$1.4^{+0.09}_{-0.90}$	$1.0^{+0.04}_{-0.15}$	$\mathbf{0.96^{+0.15}_{-0.08}}$	$0.99^{+0.08}_{-0.12}$	$0.96^{+0.30}_{-0.05}$
τ	$0.014^{+0.37}_{-0.004}$	$0.15^{+0.25}_{-0.14}$	$0.17^{+0.09}_{-0.15}$	$0.01^{+0.35}_{-0.001}$	$\mathbf{0.26^{+0.15}_{-0.08}}$	$0.28^{+0.12}_{-0.27}$	$0.014^{+0.500}_{-0.004}$
$z_{re}{}^{a}$	$3.2^{+21.7}_{-0.7}$	$16.3^{+11.5}_{-13.9}$	$17.8^{+4.9}_{-15.2}$	$2.7^{+23.5}_{-0.22}$	$\mathbf{23.8^{+5.9}_{-5.0}}$	$23.5^{+3.9}_{-21.0}$	$3.2^{+26.6}_{-0.83}$
Ω_Λ	$0.70^{+0.16}_{-0.18}$	$0.71^{+0.17}_{+0.24}$	$0.70^{+0.13}_{-0.21}$	$0.71^{+0.12}_{-0.20}$	$\mathbf{0.74^{+0.13}_{-0.10}}$	$0.75^{+0.12}_{-0.23}$	$0.65^{+0.24}_{-0.23}$
$\Omega_b h^2$	$0.022^{+0.006}_{-0.001}$	$0.023^{+0.005}_{-0.004}$	$0.024^{+0.001}_{-0.002}$	$0.023^{+0.005}_{-0.002}$	$\mathbf{0.023^{+0.004}_{-0.003}}$	$0.025^{+0.002}_{-0.005}$	$0.023^{+0.009}_{-0.002}$
$-\ln\mathcal{L}$	484.89	484.89	485.18	486.46	**483.44**	484.45	486.28
$\chi^2_{\mathrm{eff}} \equiv -2\ln\mathcal{L}$	969.78	969.78	970.36	972.92	**966.88**	968.90	972.56
d.o.f.	891	891	892	892	**890**	890	893

[†] $\varepsilon_* = 0.2$
[‡] $\varepsilon_* = 0.75$
[a] Reionization epoch as defined in [46]

likelihood values are comparable. We obtain $\varepsilon_* = 0.2$ (ES-a(VI)) by carrying out MCMC with ES(VI) model which gives the best likelihood for this model while $\varepsilon_* = 0.75$ (ES-b (VI)) gives the best shape (i.e. closest to the recovered power spectrum) but is slightly less likely. In Fig. 2 we have plotted the angular power spectrum C_l obtained using the best fit values after the MCMC analysis. We corroborate the preferred value for $k_* \sim 3 \times 10^{-4}$ Mpc^{-1} as obtained by [31] for the exponential cutoff power spectrum (EC(II)). An important difference to be noted is in the value of α. We obtain better likelihoods as the value of α increases. In fact, it can be seen from Table II that the best likelihood is obtained for a steeper exponential cutoff, i.e. $\alpha = 9.6$ ($-\ln\mathcal{L} = 485.2$ for $\alpha = 3.35$) in contrast to earlier studies [31]. This is also in good agreement with the recovered power spectrum of [24] where again a very sharp cutoff ($\alpha = 10$), gave a better fit to WMAP data.

Fig. 3 shows the mean likelihoods for k_* for the models using WMAP TT data. We note that compared to other models the probability for model ES-a(VI) is sharply peaked on $k_* \sim 3.2 \times 10^{-4}$ Mpc^{-1}. This however, does not translate to tight 1-σ error bars in the corresponding table due to the bimodal probability distribution with a smaller, broad secondary peak at low wavenumber for this model.

The values of the spectral index, n_s and cosmological constant, Ω_Λ affect the shape and the amplitude of the power spectrum of matter distribution. We would like to mention that getting the estimate of τ from the low multipoles is important to break parameter degeneracies. As more parameters are added, precision continues to reduce (unless new degeneracies are broken) as many of the parameters are correlated. Deviation in primordial spectral index n_s is a consequence of strong correlation with τ [54]. In Fig. 4 we show the correlation between the optical depth τ and the inflationary parameters, k_*, α, R_* along with the correlated n_s. We notice that the increase in τ and k_* is compensated by a corresponding increase in n_s. Therefore, we find that inflationary models such as SB(III), KD(IV), and ESa-b(VI) models (with cutoff plus 'bump') provide better fit to the observed WMAP data. Another interesting result that emerges is the difference in τ inferred with and without the WMAP polarization TE data. It is much less marked for models with infrared cutoff than for the pure Power Law model. Perhaps this could be an indirect evidence in favour of an infrared cutoff. We consider the VF model as not a very good fit to the data and leave it out of any further discussion. Table III gives the parameter search results with the external CMB datasets (CBI,
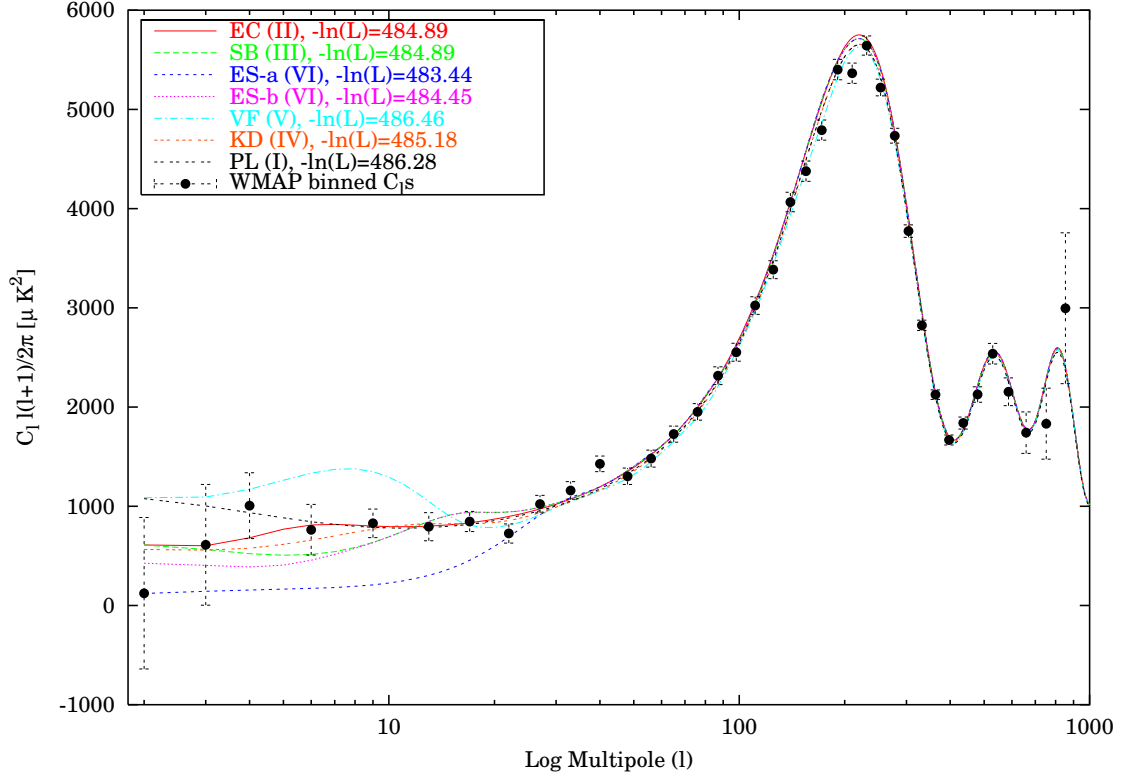
FIG. 2: The angular power spectra (C_l) for the different primordial power models along with their best fit likelihood values are given in the figure. The plot also shows the WMAP binned C_ls for comparison
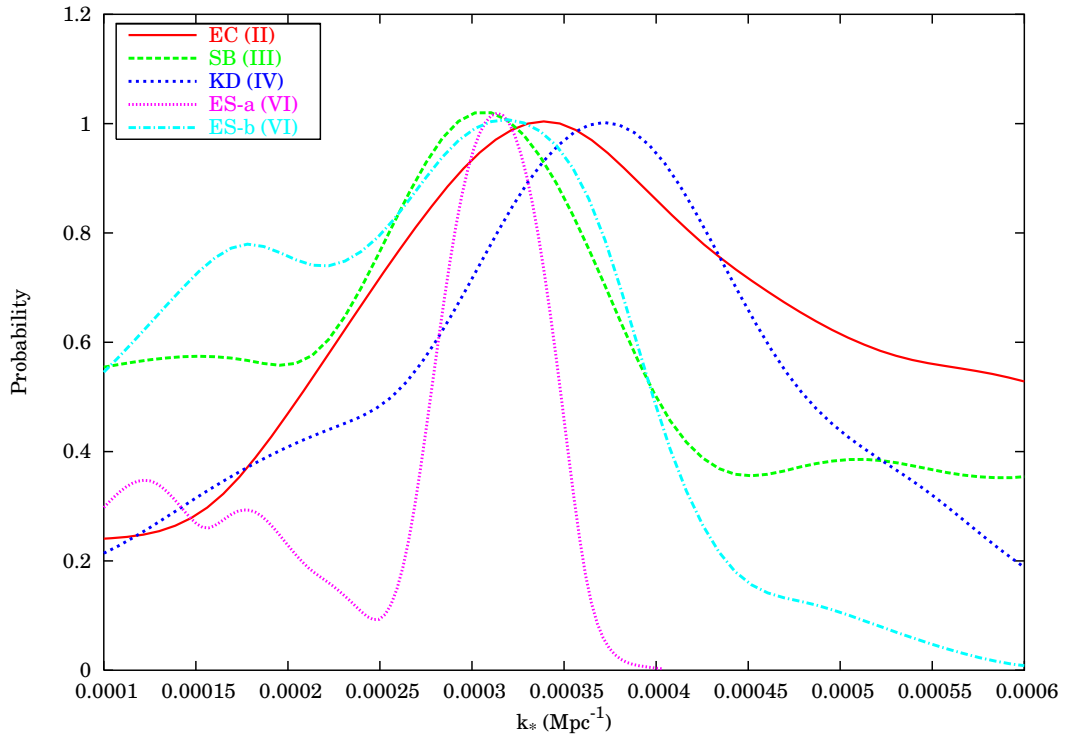
.

FIG. 3: The plot shows the mean likelihoods of the cutoff parameter, k_* obtained after performing MCMC for the models as discussed in the text using WMAP TT data. Notably, the probability for model ES-a(VI) is sharply peaked around $k_* \sim 3.2 \times 10^{-4}$ Mpc^{-1}.

TABLE III: Best fit values of parameters specifying the initial power spectrum (k_*, α, R_*, n_s) and other relevant cosmological parameters obtained using a class of model power spectra with a infrared cutoff (dataset used: WMAP (TT+TE) + External (CBI, ACBAR, VSA) CMB datasets)

Parameter	Expo-cutoff EC(II)	Starobinsky SB(III)	Kin. Dom. KD(IV)	VF VF(V)	**Expo-staro(a)[†] ES-a(VI)**	Expo-staro(b)[‡] ES-b(VI)	Power Law PL(I)
$k_* (\times 10^{-4})$ Mpc^{-1}	$2.6^{+5.2}_{-2.5}$	$8.9^{+0.1}_{-7.9}$	$3.5^{+2.9}_{-3.4}$	$0.40^{+1.7}_{-0.30}$	$\mathbf{1.2^{+1.0}_{-0.19}}$	$1.3^{+2.5}_{-0.3}$	–
α	$6.0^{+3.5}_{-4.9}$	–	–	–	$\mathbf{0.89^{+0.41}_{-0.73}}$	$0.78^{+2.4}_{-0.64}$	–
R_*	–	$0.85^{+0.14}_{-0.5}$	–	–	$\mathbf{0.017^{+0.96}_{-0.006}}$	$0.15^{+0.83}_{-0.14}$	–
n_s	$0.96^{+0.09}_{-0.04}$	$0.95^{+0.16}_{-0.06}$	$1.40^{+0.02}_{-0.97}$	$1.04^{+0.05}_{-0.11}$	$\mathbf{0.95^{+0.11}_{-0.09}}$	$0.94^{+0.15}_{-0.07}$	$0.95^{+0.19}_{-0.05}$
τ	$0.12^{+0.20}_{-0.10}$	$0.19^{+0.23}_{-0.18}$	$0.23^{+0.04}_{-0.11}$	$0.12^{+0.23}_{-0.07}$	$\mathbf{0.16^{+0.21}_{-0.09}}$	$0.12^{+0.36}_{-0.31}$	$0.11^{+0.35}_{-0.09}$
z_{re}[a]	$13.8^{+11.3}_{-10.6}$	$19.1^{+9.05}_{-16.4}$	$20.7^{+1.7}_{-7.2}$	$14.2^{+11.1}_{-6.1}$	$\mathbf{16.9^{+10.7}_{-7.6}}$	$13.6^{+16.6}_{-6.5}$	$13.1^{+14.9}_{-10.4}$
Ω_Λ	$0.74^{+0.12}_{-0.10}$	$0.78^{+0.12}_{-0.15}$	$0.80^{+0.06}_{-0.12}$	$0.73^{+0.13}_{-0.10}$	$\mathbf{0.75^{+0.10}_{-0.16}}$	$0.72^{+0.16}_{-0.11}$	$0.74^{+0.15}_{-0.12}$
$\Omega_b h^2$	$0.023^{+0.003}_{-0.002}$	$0.022^{+0.006}_{-0.003}$	$0.024^{+0.001}_{-0.002}$	$0.022^{+0.004}_{-0.002}$	$\mathbf{0.022^{+0.004}_{-0.002}}$	$0.022^{+0.005}_{-0.003}$	$0.023^{0.005}_{-0.002}$
$-\ln \mathcal{L}$	725.25	723.95	726.68	726.30	**723.36**	723.58	726.20
$\chi^2_{\mathrm{eff}} \equiv -2\ln \mathcal{L}$	1450.50	1447.90	1453.36	1452.60	**1446.72**	1447.16	1452.40
d.o.f.	1442	1442	1443	1443	**1441**	1441	1444

[†]$\varepsilon_* = 0.2$
[‡]$\varepsilon_* = 0.75$
[a]Reionization epoch as defined in [46]

ACBAR, VSA). In this case too we report the best likelihood with ESa-b(VI) $\mathcal{P}(k)$ compared to the rest of the pack. To investigate the effect of priors we performed a number of MCMC simulations with different priors within the ranges given in Table I and found that the dependence of the results on priors is weak [55].

We note that introducing a cutoff k_* and a 'bump' at low wavenumber in the primordial power spectrum provides a better fit to the observed CMB data. Such scenarios can explain the lack of power at low multipoles as shown in Fig. 2.

V. DISCUSSION AND CONCLUSION

The cosmological model and parameter constraints deduced from observations are sensitive to assumptions regarding the power spectrum of primordial density perturbations. The suppression of power in the quadrupole of the CMB anisotropy could be signaling a radical departure (in the form of an infrared cutoff) from the near-scale invariance of the primordial spectrum predicted by simplest inflationary scenarios. The very presence of a feature in the primordial spectrum indicates modification to the simplest inflationary scenarios and calls for an exploration of extensions based on plausible physical mechanisms.

We show that sharp features, such as a infrared cutoff near the horizon scale and a 'bump', in the primordial power spectrum provides a likely explanation to power suppression at low multipoles as seen in the recent WMAP data. Although a steep monotonic cutoff tends to pull down the power in the next few higher multipoles above the quadrupole and octopole but this is well compensated by the sudden excess power following the sharp rise. This allows a steep cutoff to match the low quadrupole and octopole without suppressing the higher multipoles. This is evident in the studies where the primordial power spectra was directly deconvolved from the data [24, 34]. In the light of the analysis conducted in this work we give more credence to inflationary models with cutoffs than put forth in earlier studies [30, 31]. It can be seen through this study that a break in the initial power spectrum confronts the CMB data better. This is also borne out in recent Bayesian evidence assessment of a different set of model spectra with infrared cutoff [29]. The
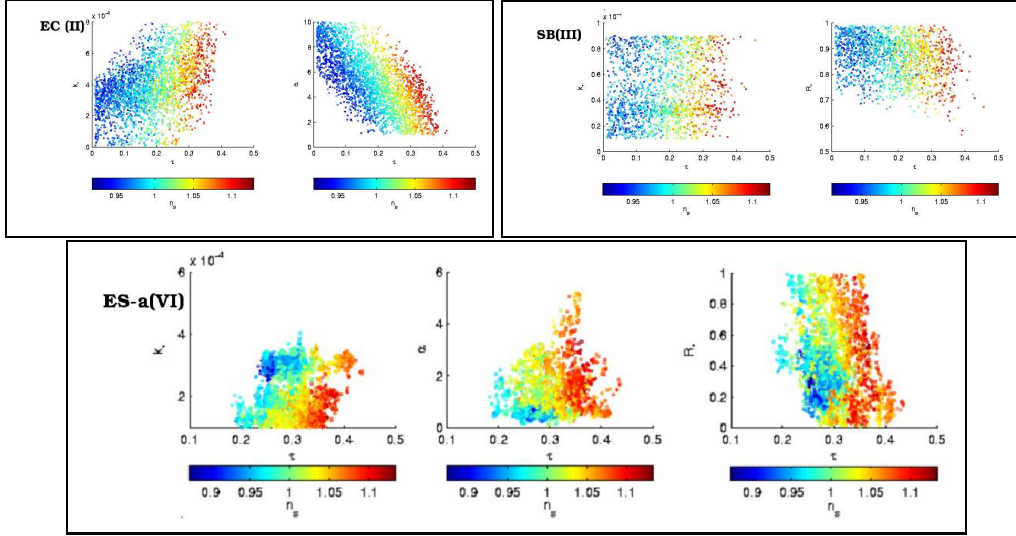
FIG. 4: The plots show the posterior distribution of the parameter τ plotted against the parameters k_* and α for exponential cutoff EC(II) model (Top left panel), k_* and R_* for Starobinksy SB(III) model (Top right panel) and k_*, α and R_* for expo-staro ES-a(VI) model (bottom panel). Points are colored according to the value of n_s.

question however, remains of the location of this cutoff. Our study suggests that a cutoff of $k_* \sim 3 \times 10^{-4}$ Mpc^{-1} with WMAP TT data and $1.1 \times 10^{-4} \leq k_* \leq 9.0 \times 10^{-4}$ Mpc^{-1} (inclusive of error bars) with all the CMB datasets. However, more detailed and wider exploration of the infrared cutoff mechanism within inflation is required. A comparison of the best fit model spectra with the recovered spectra shows that the form of infrared cutoff has substantial scope for improvement. This keeps open the pursuit of (physically motivated) mechanisms within simple inflation that produces the form of infrared cutoff suggested by the data.

Studies such as [36] also assert that the presence of such features if confirmed further by observations would be attributed to the initial power spectrum and not due to oscillations produced by any other means as suggested in Ref. [56]. Other feasible possibilities which produce such features in the initial power spectrum are the multiple-field inflationary models. Some of these have been tested with the recent observed CMB data such as the double inflation [33] scenario. However, such studies indicate that the present CMB data (WMAP first year data) strongly favour single-inflaton field models. Further discussion on the classes of inflationary models supported by observational data can only be made and asserted after future advancement in measurements, in particular, those of CMB polarization. The polarization power spectra have different parameter dependence as opposed to the temperature power spectra. This aids in breaking some parameter degeneracies. Moreover, since their source of origin is different and the polarization spectra directly probes the epoch of last scattering so polarization can be a better probe of the inflationary epoch.

[1] D. N. Spergel *et al.*, ApJS **148** 175 (2003).
[2] H. V. Peiris *et al.*, ApJS **148** 213 (2003).
[3] J. R. Bond *et al.*, Phil.Trans.Roy.Soc.Lond. A **361** 2435 (2003).
[4] C. J. MacTavish *et al.*, *preprint*, astro-ph/0507503 (2005).
[5] L. A. Kofman, A. D. Linde, A. A. Starobinsky, Phys. Lett. B **157** 361 (1985).
[6] L. A. Kofman, A. D. Linde, Nucl. Phys. B **282** 555 (1987).
[7] J. Silk, M. S. Turner, Phys. Rev. D **35** 419 (1987).
[8] L. A. Kofman and D. Y. Pogosyan, Phys. Lett. B **214** 508 (1988).

 [9] J. R. Bond and D. Salopek, Phys. Rev. D **40** 1753 (1989).
[10] V. F. Mukhanov and M. I. Zelnikov, Phys. Lett. B **263** 169 (1991).
[11] D. Polarski and A. A. Starobinsky, Nucl. Phys. B **385** 623 (1992).
[12] The quadrupole suffers the most due to the lack of power on large scales followed by the octopole to a lesser extent. In this study we have considered the overall discrepancy observed at low multipoles.
[13] Y. P. Jing and L. Z. Fang, Phys. Rev. Lett. **73** 1882 (1994).
[14] C. L. Bennett *et al.*, ApJS **148** 1 (2003).
[15] G. Hinshaw *et al.*, astro-ph/0603451 (2006).
[16] G. Efstathiou, MNRAS **343** L95 (2003).
[17] J. P. Luminet *et al.*, Nature London **425** 593 (2003).
[18] A. Hajian and T. Souradeep, Astrophys.J. Lett. **597** L5 (2003); A. Hajian, T. Souradeep, and N. Cornish, Astrophys.J. **618** L63 (2005).
[19] T. Moroi and T. Takahashi, Phys. Rev. Lett. 92, 091301 (2004).
[20] C. Gordon, W. Hu, Phys. Rev. D **70** 083003 (2004) and references therein.
[21] S. L. Bridle *et. al.*, MNRAS **342** L72 (2003).
[22] S. Hannestad, JCAP 04 (2004) 002.
[23] P. Mukherjee and Y. Wang, Astrophys.J. **599** 1 (2003).
[24] A. Shafieloo and T. Souradeep, Phys. Rev. D **70** 043523 (2004).
[25] P. Mukherjee and Y. Wang, JCAP 12 (2005) 007.
[26] Marginalization over systematic effects such as residuals from foreground removal can further reduce the significance of this discrepancy [27].
[27] A. Slosar and U. Seljak, Phys. Rev. D **70** 083002 (2004); A. Slosar *et al.*, Phys. Rev. D **69** 123003 (2004) and references therein.
[28] A. Niarchou, A. H. Jaffe and L. Pogosian, Phys. Rev. D **69** 063515 (2004).
[29] M. Bridges, A. N. Lasenby and M. P. Hobson, *preprint*, astro-ph/0511573 (2005).
[30] C. Contaldi *et al.*, JCAP **0307** 002 (2003).
[31] J. M. Cline *et al.*, JCAP **0309** 010 (2003).
[32] B. Feng, X. Zhang, Phys. Lett. B **570** 145 (2003).
[33] D. Parkinson *et. al.*, Phys. Rev. D **71** 063524 (2005).
[34] D. Tocchini-Valentini, M. Douspis, J. Silk, MNRAS **359** 31 (2005).
[35] It is interesting to recall the similarity of the equation for the generation of perturbations at a given wavenumber and harmonic oscillators. Sharp features in the power spectrum created by changes in the 'effective mass' of the perturbations are accompanied by overshoots and ringing just as in (under damped) harmonic oscillators.
[36] J. Lesgourgues *et. al.*, MNRAS **297** 769 (1998).
[37] J. Einasto *et al.*, Nature **385** 139 (1997).
[38] E. Gaztañaga and C. M. Baugh, MNRAS **294**, 229 (1998).
[39] A. Lewis, S. Bridle, Phys. Rev. D **66** 103511 (2002).
[40] The standard Richardson Lucy (RL) method can start fitting noise at large iterations and produce spurious oscillations. [24] use an improved Richardson Lucy (RL) method wherein a convergence function is used to weigh down the contribution of noise and sample variance along with a smoothening function (details in [24]). In this work the plot given in Fig. 1 (Recovered (sm)) is a further improvement over [24] (Fig. 1 (Recovered)) as it is wavelet smoothed. Such procedure removes any spurious oscillations of the standard RL method giving credence to the features detected by the improved method ([24] has been cited in the WMAP 3-year paper [15]) .
[41] Although these can be treated under the same class of inflationary models but for the sake of clarity we will hereafter refer to these different forms as different models.
[42] A. A. Starobinsky, JETP Lett. **55** 489 (1992) [Pisma Zh. Eksp. Teor. Fiz. **55** 477 (1992)].
[43] A. Vilenkin and L. H. Ford, Phys. Rev. D **26** 1231 (1982).
[44] Radford Neal's Research: Markov Chain Monte Carlo: http://www.cs.toronto.edu/ radford/res-mcmc.html.
[45] The Hubble parameter is expressed in terms of the angular scale subtended by acoustic horizon at last scattering i.e. θ ($= r_s/D_a$, i.e. the ratio of the sound horizon, r_s to the angular diameter distance to the last scattering surface, D_a).
[46] The redshift at reionization z_{re} is not a free parameter here but a parameter derived from τ related by $\tau = \sigma_T \int_0^{z_{re}} dz\, n_e(z)/[(1+z)^2 H(z)]$, where n_e is the number density of electrons and σ_T is the Thompson scattering cross-section, assuming rapid reionization [39].
[47] In a single scalar field potential with infrared cutoffs the contribution to low multipole TT data from tensor modes is small (J. Lasue and T. Souradeep-*unpublished*)), hence we have not taken into account the tensor spectral index, n_t.
[48] A_s is the primordial superhorizon power in the curvature perturbation on 0.05 Mpc^{-1} scales.
[49] N. Metropolis, *et. al.* J. Chem. Phys. **21** 1087 (1953).
[50] R. M. Neal, Annals of Statistics **31** 3 705 (2003); David J. C. MacKay Information Theory, Inference, and Learning Algorithms (online version of book) Chap 29, 374 (2003).
[51] L. Verde *et al.*, ApJS **148** 195 (2003).
[52] C. R. Contaldi *et al.* Phys. Rev. Lett bf 90 221303 (2003).
[53] D. N. Spergel *et al.*, astro-ph/0603449; *Submitted to Astrophys.J.* (2006).
[54] P. Bernardis *et al.*, Astrophys.J. **564** 559 (2002).

[55] A. Slosar *et al.* MNRAS 341, L29 (2003).
[56] F. Atrio-Barandela *et al.* JETP Lett. **66** 397 (1997).